

Experimental long-lived entanglement of two macroscopic objects.

Brian Julsgaard, Alexander Kozhekin, and Eugene S. Polzik

Institute of Physics and Astronomy, University of Aarhus, 8000 Aarhus, Denmark

Entanglement is considered to be one of the most profound features of quantum mechanics^{1,2}. An entangled state of a system consisting of two subsystems cannot be described as a product of the quantum states of the two subsystems^{9,10,16,17}. In this sense the entangled system is considered inseparable and nonlocal. It is generally believed that entanglement manifests itself mostly in systems consisting of a small number of microscopic particles. Here we demonstrate experimentally the entanglement of two objects, each consisting of about 10^{12} atoms. Entanglement is generated “on demand” via interaction of the two objects - more precisely, two gas samples of cesium atoms - with a pulse of light, which performs a non-local Bell measurement on collective spins of the samples¹⁴. The entangled spin state can be maintained for 0.5 millisecond, contrary to the popular belief that entanglement in a multi-particle system decays almost instantaneously due to decoherence effects. Besides being of fundamental interest, the robust, long-lived entanglement of material objects demonstrated here is expected to be useful in quantum information processing, including teleportation³⁻⁵ of quantum states of matter and quantum memory.

In 1935 Einstein, Podolsky and Rosen (EPR) published a famous paper¹ formulating what they perceived as a paradox created by quantum mechanics. Since then, the EPR correlations and other types of entanglement have been extensively analyzed with seminal contributions made by J. Bell². Entangled or inseparable states are fundamental to the field of quantum information, specifically to quantum teleportation of discrete^{3,4} and continuous⁵ variables and to quantum dense coding of discrete⁶ and continuous^{7,8} variables, to name a few examples. The majority of experiments on entanglement to date deal with entangled states of light^{3-6,9-11}. Entangled states of discrete photonic variables (spin $\frac{1}{2}$ systems)^{9,10} as well as entangled states of continuous variables (quadrature-phase operators) of the electro-magnetic field¹¹ have been generated experimentally. Entangled states of material particles are much more difficult to generate experimentally; however, such states are vital for storage and processing of quantum information. Recently, entangled states of four trapped ions have been produced¹², and two atoms have been entangled via interaction with a microwave photon field¹³.

In this Letter we describe an experiment on the generation of entanglement between two separate samples of atoms containing 10^{12} atoms each, along the lines of a recent proposal¹⁴. Besides the fact that we demonstrate a quantum entanglement at the level of macroscopic objects, our experiment proves feasible a new approach to the quantum interface between light and atoms suggested in^{14,15} and paves the road towards the other protocols proposed there, such as the teleportation of atomic states and quantum memory. A distinctive feature of our approach is that the entanglement is generated through a non-local Bell measurement on the two samples' spins performed by transmitting a pulse of light through the samples. No other interaction between the samples is required, which means that the two samples can be positioned at a considerable distance from each other.

The ideal EPR entangled state of two sub-systems described by continuous non-commuting variables $\hat{X}_{1,2}$ and $\hat{P}_{1,2}$, e.g., positions and momenta of two particles, is the state for which $\hat{X}_1 + \hat{X}_2 \rightarrow 0, \hat{P}_1 - \hat{P}_2 \rightarrow 0$. Recently in^{16,17}, the necessary and sufficient condition for the entanglement or inseparability for such quantum variables has been cast in a form of the following inequality involving the variances of the sum/difference of the positions/momenta for the two systems: $\langle (\delta(\hat{X}_1 + \hat{X}_2))^2 \rangle + \langle (\delta(\hat{P}_1 - \hat{P}_2))^2 \rangle < 2$. In our experiment the quantum variables analogous to the position and momentum operators are two projections of the collective spin (total angular momentum) of an atomic sample. The analogy is evident from the commutation relation $[\hat{J}_z, \hat{J}_y] = i\hat{J}_x$, which can be rewritten as $[\hat{X}, \hat{P}] = i$, where $\hat{X} = \hat{J}_z / \sqrt{J_x}$ and $\hat{P} = \hat{J}_y / \sqrt{J_x}$ if the atomic sample is spin-polarized along the x axis with \hat{J}_x having a large classical value J_x . For two spin-polarized atomic samples with $J_{x1} = -J_{x2} = J_x$ the above entanglement condition translates into

$$\delta J_{12}^2 \equiv \delta J_{z12}^2 + \delta J_{y12}^2 < 2J_x \quad (1)$$

where we introduce the notations $\delta J_{z12}^2 = \langle (\delta(\hat{J}_{z1} + \hat{J}_{z2}))^2 \rangle, \delta J_{y12}^2 = \langle (\delta(\hat{J}_{y1} + \hat{J}_{y2}))^2 \rangle$. The interpretation of condition (1) comes from the recognition of the fact that for both atomic samples in coherent spin states (CSS) the equality $\delta J_{y,z}^2 = 1/2 J_x$ holds. This equality leads to the upper bound of the condition (1). A CSS is characterized by uncorrelated individual

atoms^{18,19}. Entanglement between atoms of the two samples is, therefore, according to (1) equivalent to the spin variances smaller than that for samples in a CSS.

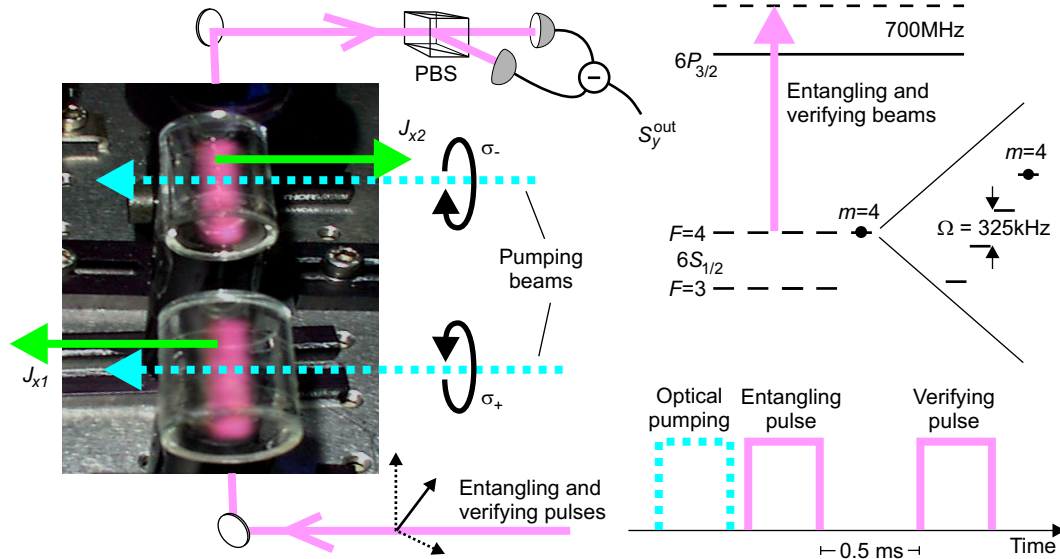


Figure 1. Schematic of the experimental setup, atomic level structure and the sequence of optical pulses. Fluorescence of atoms interacting with light is seen inside the cells (artificial colour).

Entanglement of atoms in our experiment is produced via interaction of atoms with polarized light. Quantum mechanically, a polarized pulse of light is described by Stokes operators obeying the same commutation relation as spin operators, $[\hat{S}_y, \hat{S}_z] = i\hat{S}_x$. \hat{S}_x is the difference between photon numbers in x and y linear polarizations, \hat{S}_y is the difference between polarizations at $\pm 45^\circ$, and \hat{S}_z is the difference between the left- and right-hand circular polarizations along the propagation direction, z . In our experiment light is linearly polarized along the x axis and propagates along the z axis. Hence the two pairs of continuous quantum variables engaged in the entanglement protocol are \hat{J}_z and \hat{J}_y for atoms and \hat{S}_z and \hat{S}_y for light.

In this Letter we report on the generation of the entangled state of two separate cesium gas samples (Fig. 1), which obey the entanglement condition (1).

The basics of the entanglement protocol follow the proposal¹⁴. As shown in^{14,15}, when an off-resonant pulse is transmitted through two atomic samples with opposite mean spins $J_{x1} = -J_{x2} = J_x$, the light and atomic variables evolve as

$$\begin{aligned}\hat{S}_y^{out} &= \hat{S}_y^{in} + \alpha \hat{J}_{z12}, \hat{S}_z^{out} = \hat{S}_z^{in} \\ \hat{J}_{y1}^{out} &= \hat{J}_{y1}^{in} + \beta \hat{S}_z^{in}, \hat{J}_{y2}^{out} = \hat{J}_{y2}^{in} - \beta \hat{S}_z^{in}, \hat{J}_{z1}^{out} = \hat{J}_{z1}^{in}, \hat{J}_{z2}^{out} = \hat{J}_{z2}^{in}\end{aligned}\quad (2)$$

According to (2), the measurement of \hat{S}_y^{out} reveals the value of $\hat{J}_{z12} = \hat{J}_{z1} + \hat{J}_{z2}$ (provided the constant α is large enough, so that \hat{S}_y^{in} is a relatively small term) without changing this value. It follows from (2) that the total y spin projection for both samples is also conserved, $\hat{J}_{y1}^{out} + \hat{J}_{y2}^{out} = \hat{J}_{y1}^{in} + \hat{J}_{y2}^{in}$ ¹⁴. Now the spins can be rotated to interchange the spin components $z \leftrightarrow y$ and the procedure can be repeated with another pulse of light measuring the sum of y components, $\hat{J}_{y1} + \hat{J}_{y2}$, again in a non-demolition way, while at the same time leaving the previously measured value of $\hat{J}_{z1} + \hat{J}_{z2}$ intact. As a result, the sum of the z components and the sum of the y components of spins of the two samples are known exactly in the ideal case, and therefore the two samples are entangled according to (1), since the uncertainties on the left-hand side become negligible.

An important modification of the above protocol is the addition of a magnetic field oriented along the direction x , which allows to use a single entangling pulse to measure both z and y . The Larmor precession of the J_z, J_y components with a common frequency Ω does not change their mutual orientation and size and therefore does not affect the entanglement. On the other hand, the precession allows us to extract information about both z and y components from a single probe pulse as described below. Moreover, in the lab frame the spin state is now encoded at the frequency Ω , and as usual an ac measurement is easier to reduce to the quantum noise level than a dc measurement. Measurements of the light noise can be now conducted only around its Ω spectral component. By choosing a suitable radio-frequency value for Ω we can reduce the probe noise $\hat{S}_{y,z}^{in}(\Omega)$ to the minimal level of the vacuum (shot) noise. In the presence of the magnetic field the spin behavior is described by the following equations: $\dot{\hat{J}}_z(t) = \Omega \hat{J}_y(t), \dot{\hat{J}}_y(t) = -\Omega \hat{J}_z(t) + \beta \dot{\hat{S}}_z(t)$, whereas the Stokes operators still evolve according to equation (2). Solving the spin equations and using (2) we obtain

$$\hat{S}_y^{out}(t) = \hat{S}_y^{in}(t) + \alpha \left\{ \hat{J}_{z12} \cos(\Omega t) + \hat{J}_{y12} \sin(\Omega t) \right\} \quad (3)$$

The $\hat{J}_{z,y}$ components are now defined in the frame rotating with the frequency Ω around the magnetic field direction x . It is clear from (3) that by measuring the $\cos(\Omega t)/\sin(\Omega t)$ component of $\hat{S}_y^{out}(t)$ one acquires the knowledge of the z/y spin projections. Simultaneous measurement of both spin components of the two atomic samples is possible because they commute, $[\hat{J}_{z1} + \hat{J}_{z2}, \hat{J}_{y1} + \hat{J}_{y2}] = i(J_{x1} + J_{x2}) = 0$.

The schematic of the experimental set-up is shown in Fig. 1. The two atomic samples in glass cells 3*3cm at approximately room temperature are placed in a highly homogenous magnetic field of 0.9 Gauss ($\Omega = 325kHz$) surrounded by a magnetic shield. Cesium atoms are optically pumped into $F = 4, m_F = 4$ ground state in the first cell and into $F = 4, m_F = -4$ in the second cell to form coherent spin states oriented along x axis for cell 1 and along $-x$ for cell 2. Optical pumping is achieved with circularly polarized 500μ sec pulses at $852nm$ and $894nm$ with opposite helicity for the two cells. The mean spin value for each sample is given by $J_x = N \sum_{m=-4}^4 m \rho_{mm} = 4Np \rightarrow 4N$, with the limiting value corresponding to a perfect spin polarization, $p = 1$. The $|J_x|$ for the two cells is adjusted to be equal to better than 10%. The cells are coated from inside with a paraffin coating which enhances the ground state orientation life time T_2 up to $30m$ sec. This long T_2 leads to a long storage time of a spin state. The $|J_x|$, T_2 and p are measured by the magneto-optical resonance method.

After the samples are prepared in CSS, optical pumping is switched off and a probe pulse is sent through. It is an off-resonant pulse blue-detuned by $\Delta = 700MHz$ from the closest hyperfine component of the D_2 line at $852nm$. Its Stokes operator S_y is measured by a polarizing beam splitter with two balanced detectors. The differential photocurrent from the detectors is split in two and its $\cos(\Omega t)$ and $\sin(\Omega t)$ power spectral components $(S_{yCos}^{out}(\Omega))^2$ and $(S_{ySin}^{out}(\Omega))^2$ are measured by lock-in amplifiers. Repeating this sequence many times we obtain the variances for these components, in short, spectral variances, which according to eq.(3) are $(\delta S_{yCos}^{out}(\Omega))^2 = (\delta S_{yCos}^{in}(\Omega))^2 + \frac{1}{2} \alpha^2 \delta \hat{J}_{z12}^2 \equiv \frac{1}{2} \delta S^2 + \kappa \delta J_{z12}^2$ and similarly for

$(\delta S_{y\sin}^{out}(\Omega))^2$ with substitution $J_z \rightarrow J_y$. The coefficient $\alpha = \sigma\gamma n / A\Delta$ ¹² along with the value $|J_x|$ determines the ratio of the atomic state term and the light state term. σ is the resonant dipole crosssection, $\gamma = 2.5\text{MHz}$ - the half-width of the optical transition, $A = 2\text{cm}^2$ - the probe beam crosssection, and n - the number of photons in the probe pulse. A typical probe power is around 5mW .

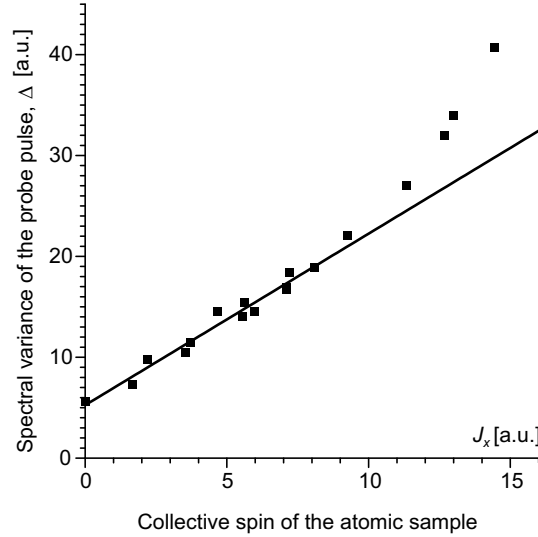


Figure 2. Determination of the coherent spin state limit for entanglement. Linear fit to the experimental data at low values of J_x corresponds to the CSS limit. Spin orientation is better than 95%. Non-zero variance at $J_x = 0$ is due to the probe noise. Deviation from the CSS limit at higher atomic densities is due to quadratic contribution of the classical spin noise.

The total measured variance of the two quadratures of the photocurrent

$$\Delta = (\delta S_{y\cos}^{out}(\Omega))^2 + (\delta S_{y\sin}^{out}(\Omega))^2 = \delta S^2 + \kappa\delta J_{z12}^2 + \kappa\delta J_{y12}^2 \equiv \delta S^2 + \kappa\delta J_{12}^2$$

is plotted in Fig. 2 as a function of J_x , which is varied by heating the cells and by adjusting optical pumping. In the absence of atoms in the cells the measured spectral variance is due to the initial probe state variance δS^2 . δS^2 is at the vacuum (shot) noise level, which has been verified experimentally by checking its characteristic linear dependence on the probe power. As seen in the Fig. 2, with atoms present the measured variance grows linearly with J_x at low densities, which proves that the observed atomic fluctuations at these densities are due to quantum atomic noise²⁰. The

degree of the spin polarization for the data in Fig. 2 is nearly perfect, $p \geq 95\%$. We therefore conclude that a linear fit to the observed data corresponds to the CSS of both atomic samples with $\delta J_{12}^2 = 2J_x$ and hence this line, which we denote by $\Delta(J_x)$, establishes the noise level corresponding to the right hand side of the inequality (1). Deviations of the observed variance from the linear fit at higher atomic numbers are due to the nonlinearly growing contribution of classical technical noise of the spin state because of the technical noise of lasers, the non-ideal cancellation of the back action of the probe on the two samples, etc.

The entanglement condition (1) can be re-written in experimentally measured quantities, including the noise of the probe, as

$$\delta S^2 + \kappa \delta J_{12}^2 < \delta S^2 + 2\kappa J_x = \Delta(J_x) \quad (4)$$

The final measurement sequence aimed at the generation and verification of the entanglement consists of the optical pumping pulses preparing samples in a CSS, the *entangling* pulse preparing the samples in the entangled state (pulse I) and the *verifying* pulse coming after the delay time τ and verifying the entanglement (pulse II). These pulses have the same duration and optical frequency as the probe pulse used for the CSS measurements. Between the two pulses the joint spin state of the two samples evolves freely and is subject to decoherence. The photocurrents from the two pulses are subtracted electronically and the variance of the difference, Δ_{EPR} , is measured. The vanishing Δ_{EPR} corresponds to two repeated measurements on the total spin state of the two samples producing the same results, i.e. to a perfect knowledge of both \hat{J}_{z12} and \hat{J}_{y12} and therefore to a perfectly entangled state. In a non-ideal experimental case Δ_{EPR} can be expressed using (3) as

$$\begin{aligned} \Delta_{EPR} &= \delta \bar{S}_{Cos}^2 + \delta \bar{S}_{Sin}^2 \equiv \left(\delta S_{yCos}^{Iout}(\Omega) - \delta S_{yCos}^{IIout}(\Omega) \right)^2 + \left(\delta S_{ySin}^{Iout}(\Omega) - \delta S_{ySin}^{IIout}(\Omega) \right)^2 = \\ &= \delta S_{II}^2 + \kappa \left\{ \kappa^{-1} \delta S_I^2 + \left(\delta(\hat{J}_{z12})_I - \delta(\hat{J}_{z12})_{II} \right)^2 + \left(\delta(\hat{J}_{y12})_I - \delta(\hat{J}_{y12})_{II} \right)^2 \right\} \equiv \\ &\equiv \delta S_{II}^2 + \kappa \delta J_{EPR}^2 \end{aligned} \quad (5)$$

The variance δJ_{EPR}^2 determines the uncertainty of the spin components of the state prepared by the entangling pulse and measured after the time τ . It contains two contributions, δS_I^2 due to the quantum noise of the entangling pulse, and all other terms in curly brackets, which are due to decoherence during the time τ . The verifying pulse in our experiment is also not noiseless

and therefore its variance, δS_{II}^2 , also contributes to Δ_{EPR} . In the experiment

$\delta S_I^2 = \delta S_{II}^2 = \delta S^2$. The exact entanglement condition, $\Delta_{EPR} < \Delta(J_x)$, is obtained by substituting (5) into (4). The degree of entanglement can be defined as

$$\xi = 1 - \frac{\delta J_{EPR}^2}{2J_x} = 1 - \frac{\Delta_{EPR} - \delta S^2}{\Delta(J_x) - \delta S^2}$$
. ξ varies from 0 (separable state) to 1 (perfect entanglement).

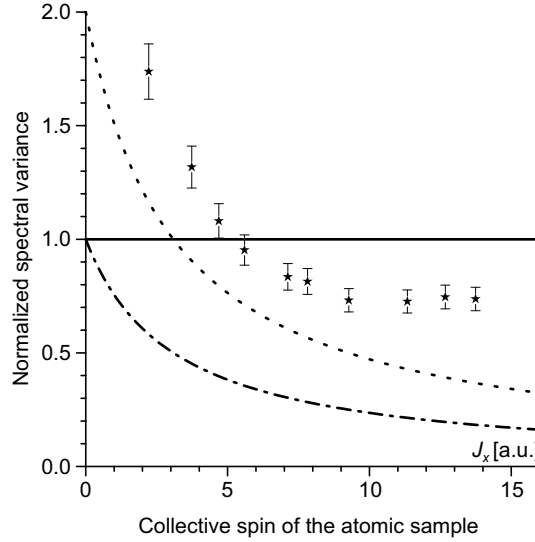


Figure 3. Demonstration of the entangled spin state for two atomic samples. All data are normalized to the coherent spin state (CSS) limit. Solid line – CSS limit – the boundary between entangled (below the line) and separable states. Experimental points – data for the entangled spin state. Dashed curve – lower limit for the entangled state variance. Dashed-dotted curve – verifying pulse quantum noise level.

The results of measurements with $\tau = 0.5m$ sec are shown in Fig. 3. The results are plotted as a function of J_x and are normalized to the CSS limit $\Delta(J_x)$ (the linear fit in Fig. 2). This limit thus corresponds to the unity level in Fig. 3. The raw experimental data $\Delta_{EPR} / \Delta(J_x)$ for the entangled state are shown as stars. The values below the unity level verify that the entangled state of the two atomic samples has been generated and maintained for $0.5m$ sec. The minimal possible level for $\Delta_{EPR} / \Delta(J_x)$ (maximum possible entanglement) is equal to $2\delta S^2 / \Delta(J_x)$ (dashed line), i.e. it is set by the total quantum noise of the two pulses. The degree of entanglement ξ is calculated using the normalized shot noise level of the

verifying pulse, $\delta S^2 / \Delta(J_x)$ (dashed-dotted line). The highest observed degree of entanglement is $\xi = (35 \pm 7)\%$.

The imperfect entanglement comes from several factors. Firstly, the vacuum noise of the entangling pulse prohibits a perfect preparation of the spin state. This is the prime reason for the absence of entanglement for the small number of atoms in the left part of the graph. Secondly, the deviation of the initial spin state from CSS, which is due to the classical noise of the lasers, becomes more pronounced as the number of atoms grows. That is why entanglement is best at intermediate atomic densities. Finally, losses of light on the way from one cell to another, as well as the spin state decay between the two measurements due to decoherence caused by quadratic Zeeman splitting and collisions preclude perfect entanglement at all atomic densities. Measurements with delay times longer than 0.8m sec demonstrate no entanglement.

Note that the atomic motion is not an obstacle in this experiment but is rather helpful. The probe beam covers most of but not the whole volume of the atomic sample, but the duration of the pulses is longer than the transient time of an atom across the cell. Therefore each light pulse effectively interacts with and entangles all atoms of the samples. In addition, a large detuning of the probe makes the Doppler broadening insignificant.

It is instructive to analyze the difference between the degree of entanglement and the degree of classical correlations for the atomic spins of the two samples. For uncorrelated atomic samples the normalized variance of the difference between the two photocurrents would be equal to 2 in notations of Fig.3. The pure atomic part of this variance V_{uncorr} would be the difference between 2 and the dashed line, i.e. would be equal to approximately 1.5 for medium atomic densities. For the actual data in Fig. 3 the difference between the experimental points and the dashed line is approximately $V_{corr} = 0.25$. The degree of correlation, defined as

$1 - \frac{V_{corr}}{V_{uncorr}}$, is 83% for this example. This number is much higher than the highest degree of entanglement reported above implying that entanglement requires something much stronger than classical correlations. The reason for this difference is that in quantum mechanics the measuring device (light in this case) becomes entangled with the measured object and therefore the noise of these two subsystems cannot be treated independently.

In conclusion, we have demonstrated on-demand generation of entanglement of two separate macroscopic objects. We have also demonstrated that this entanglement can be

maintained for more than $0.5m$ sec . The long storage time of this multi-particle entanglement is due to a high symmetry of the generated state. Any two atoms of the two samples are practically uncorrelated; entanglement manifests itself only in the collective properties of the two ensembles. Therefore a loss of coherence for a single atom makes a negligible effect on the entanglement, unlike, e.g., in the case of maximally entangled multi-particle state which is ruined by the loss of a single particle. The entanglement is generated by means of light propagating through the two samples and therefore the samples can be rather distant, provided that losses of light between them are not too high. The off-resonant character of the interaction used for the creation of entanglement allows for the potential extension of this method to other media, possibly including solid state samples with long lived spin states.

Acknowledgements: We gratefully acknowledge the contributions of J. L. Sørensen, J. Hald, A. Verchovski and C. Schori. We are also grateful to A. Kuzmich and A. Sørensen for useful discussions.

References.

1. Einstein A., Podolsky B. & Rosen N., Can quantum-mechanical description of physical reality be considered complete? *Phys. Rev.* **47**, 777-780 (1935).
2. Bell J. S., *Speakable and Unspeakable in Quantum Mechanics*. Cambridge University Press, 1988.
3. Bouwmeester, D., Pan, J. W., Mattle, K., Eibl, M., Weinfurter, H. & Zeilinger, A. Experimental quantum teleportation. *Nature*, **390**, 575 (1997)
4. Boschi, D., Branca, S., De Martini, F., Hardy & L., Popescu, S. Experimental realization of teleporting an unknown pure quantum state via dual classical and Einstein-Podolsky-Rosen channels. *Phys. Rev. Lett.*, **80**, 1121 (1998).
5. Furusawa, A., Sørensen, J. L., Braunstein, S. L., Fuchs, C. A., Kimble, H. J. & Polzik, E. S. Unconditional quantum teleportation. *Science*, 282, 706-709 (1998).
6. Mattle, K., Weinfurter, H., Kwiat, P.G. & Zeilinger, A. Dense coding in experimental quantum communication. *Phys. Rev. Lett.*, **76**, 4656-4659 (1996)
7. Braunstein, S. L. & Kimble, H. J. Dense coding for continuous variables. *Phys. Rev. A* **6104**, 2302 (2000).
8. Ban, M. Quantum dense coding via a two-mode squeezed-vacuum state. *J. Opt. B-Quantum Semicl. Opt.* **1**, L9-L11 (1999)

9. Aspect, A., Dalibard, J. & Roger, G. Experimental test of Bell's inequalities using time-varying analyzers. *Phys. Rev. Lett.*, **49**, 1804-1807 (1982).
10. Torgerson, J.R., Branning, D., Monken, C.H. & Mandel, L. Experimental demonstration of the violation of local realism without Bell inequalities. *Phys. Letters A*. **204**, 323-328 (1995).
11. Ou, Z.Y., Pereira, S.F., Kimble, H.J. & Peng, K.C. Realization of the Einstein-Podolsky-Rosen paradox for continuous variables. *Phys. Rev. Lett.* **68**, 3663-3666 (1992).
12. Sackett, C.A., Kielpinski, D., King, B.E., Langer, C., Meyer, V., Myatt, C.J., Rowe, M., Turchette, Q.A., Itano, W.M., Wineland, D.J., Monroe, I.C. Experimental entanglement of four particles. *Nature*. **404**, 256-259 (2000).
13. Rauschenbeutel, A., Nogues, G., Osnaghi, S., Bertet, P., Brune, M., Raimond, J.M. & Haroche, S., Step-by-step engineered multiparticle entanglement. *Science* , **288**, 2024-2028 (2000).
14. Duan, L.M., Cirac, J.I., Zoller, P. & Polzik, E.S. *Phys. Rev. Lett.* **85**, 5643-5646 (2000).
15. Kuzmich, A. & Polzik, E.S. Atomic quantum state teleportation and swapping. *Phys. Rev. Lett.* **85**, 5639-5642 (2000).
16. Duan, Lu.M., Giedke, G., Cirac, J.I. & Zoller, P. Inseparability criterion for continuous variable systems. *Phys. Rev. Lett.* **84**, 2722-2725 (2000).
17. Simon, R. Peres-Horodecki separability criterion for continuous variable systems. *Phys. Rev. Lett.* **84**, 2726-2729 (2000).
18. Kitagawa, M. & Ueda, M. Spin squeezed states. *Phys. Rev. A*. **47**, 5138-5143 (1993).
19. Wineland, D.J., Bollinger, J.J., Itano, W.M., Moore, F.L. & Heinzen, D.J. Spin squeezing and reduced quantum noise in spectroscopy. *Phys. Rev. A*. **46**, R6797-R6800 (1992).
20. Hald, J., Sørensen, J. L., Schori, C. & Polzik, E. S. Spin squeezed atoms: a macroscopic entangled ensemble created by light. *Phys. Rev. Lett.*, **83**, 1319-1322 (1999).

